Applied Surface Science 392 (2017) 391–401

Contents lists available at ScienceDirect

Applied Surface Science

journal homepage: www.elsevier.com/locate/apsusc

Perspective Article

Synthesis and application of iron and zinc doped biochar for removal of *p*-nitrophenol in wastewater and assessment of the influence of co-existed Pb(II)

Pei Wang[a,b], Lin Tang[a,b,*], Xue Wei[a,b], Guangming Zeng[a,b,*], Yaoyu Zhou[a,b,c], Yaocheng Deng[a,b], Jingjing Wang[a,b], Zhihong Xie[a,b], Wei Fang[a,b]

[a] College of Environmental Science and Engineering, Hunan University, Changsha 410082, China
[b] Key Laboratory of Environmental Biology and Pollution Control, Hunan University, Ministry of Education, Changsha 410082, Hunan, China
[c] College of Resources and Environment, Hunan Agricultural University, Changsha 410128, China

ARTICLE INFO

Article history:
Received 4 July 2016
Received in revised form 14 August 2016
Accepted 12 September 2016
Available online 14 September 2016

Keywords:
Iron and zinc doped biochar
p-Nitrophenol
Pb(II)
Adsorption
Complexing-bridging

ABSTRACT

The modification of biochar as a low-cost adsorbent is essential to improve its surface properties and shows great potential in water decontamination. The iron and zinc doped sawdust biochar (Fe/Zn-biochar) with large apparent surface area (518.54 m^2/g) proposed in this work showed good performance for *p*-nitrophenol (PNP) removal compared with the pristine biochar (P-biochar), iron doped biochar (Fe-biochar) and zinc doped biochar (Zn-biochar) respectively. The batch experiments turned out that Fe/Zn-biochar exhibited larger PNP adsorption capacity under acidic pH solution, and the ionic strength had slightly negative impact on PNP adsorption. The adsorption kinetics and isotherms were discussed, and the experimental data fitted well the Pseudo-second-order equation and Langmuir model. The thermodynamic study indicated that the PNP adsorption was a spontaneous endothermic process. Furthermore, the simultaneous removal for PNP and Pb(II) by Fe/Zn-biochar was investigated. It implied that the adsorption of PNP and Pb(II) at their low concentration might be enhanced by the complexing-bridging mechanism of PNP and Pb(II) ascribing to the affinity between PNP and hydrophobic sites, in addition to the affinity between Pb(II) and oxygen-containing hydrophilic sites on Fe/Zn-biochar surface. However, the predominated competition between PNP and Pb(II) at their high concentrations with Fe/Zn-biochar suppressed their adsorption.

1. Introduction

Large amount of biomass like agriculture wastes, waste sawdust, sewage sludge, and etc. are easily available. To convert them to biochar through incomplete combustion operations, such as pyrolysis and carbonization, was one of the resource utilization methods. Nowadays, the utilization of biochar as a low-cost adsorbent for pollution remediation was drawing much attention, such as for phenolic compounds and heavy metals removal in wastewater [1–3]. And the phenolic compounds adsorption process by biochar mainly contains several interaction mechanisms: (1) hydrophobic interaction, (2) hydrogen bond, (3) π-π dispersion interaction, (4) electrostatic attraction and repulsion forces [4,5].

To enhance the adsorption effect of pristine biochar, the modification of biochar was essential to improve its surface properties, such as apparent surface area, effective functional groups, hydrophobic/hydrophilic property, or surface charge [6,7]. The addition of zinc to functional materials has been studied for contaminant removal before, and the results indicated that it could help form hydroxyl groups on the surface of the ZnO particles during the preparation process [8], which was beneficial for heavy metals and organic contaminants removal [9,10]. In addition, the simultaneously introduction of iron to biochar could give rise to magnetism on the modified biochar, so the magnetic adsorbent could be easily separated from aqueous solution under a proper external magnetic field and the secondary pollution could be avoid [11].

p-Nitrophenol (PNP), as a kind of phenolic compounds, is toxic and refractory [12]. A large amount of PNP have been discharged into wastewater due to its wide application in agriculture, dyestuff and plastic industry, etc. and may cause serious harm to the

* Corresponding authors at: College of Environmental Science and Engineering, Hunan University, Changsha 410082, China.
E-mail addresses: tanglin@hnu.edu.cn (L. Tang), zgming@hnu.edu.cn (G. Zeng).

http://dx.doi.org/10.1016/j.apsusc.2016.09.052
0169-4332/

environment and human health because of its mutagenic potential and the possible damage on liver and kidney [13,14]. So, an efficient method is in urgent to control the PNP pollution from effluents before its entering into surface waters. Various methods like adsorption [15,16], reduction [13,17], catalytic degradation [12], biodegradation [14], advanced oxidation processes [18], electrochemical methods [19], and etc. have been applied to remove PNP in aqueous solution previously. While a synthetic consideration of economic feasibility, removal efficiency, the simplicity and safety of the treatment process was taken into account, the adsorption technology was a priority choice among these treatment methods [20]. Furthermore, many materials like resin [21], activated carbon [16], carbon nanosphere [22], zeolite [23], etc. have been used as adsorbents for PNP removal, but some defects like high cost, low efficiency or difficulty in solid-liquid separation, etc. exist there. So, the modified biochar as a low-cost adsorbent with large surface area and abundant functional groups was a good choice for PNP removal.

In this study, the iron and zinc doped biochar was synthesized for the first time through the thermal pyrolysis of wood waste under N_2 atmosphere, and various characterization techniques, such as the scanning electron microscopy (SEM), nitrogen adsorption-desorption isotherms, vibrating sample magnetometer (VSM), Fourier transform infrared spectrometer (FTIR), X-ray diffractometer (XRD), X-ray photoelectron spectroscopy (XPS) and zeta-potential were conducted to illustrate physicochemical properties of the resultant adsorbent and help explain its adsorption characteristics for contaminants. The prepared adsorbent was applied to remove PNP in aqueous solution here, and batch experiments were conducted to investigate the influence of pH, contact time, temperature and ionic strength on PNP adsorption. All of the adsorption kinetics, isotherms, and thermodynamics were analyzed to help explain its adsorption mechanism. Furthermore, the toxic Pb(II) may coexist with phenolic compounds in specific wastewater [21,24], and the binary system was conducted for their simultaneously removal and to study the influence of their mutual interaction on the adsorption of those two contaminants, respectively.

2. Materials and methods

2.1. Materials

The wood waste was from a timber mill in Changsha, China. The dried raw material was pulverized to obtain the fine sawdust for biochar preparation. All reagents used here including HCl, NaOH, NaCl, $ZnCl_2$, $FeCl_3\ 6H_2O$, $Pb(NO_3)_2$ and PNP were of analytical grade and provided by Shanghai Chemical Corp, China, and high-purity water (18.25 MΩ/cm) from a Millipore Milli-Q water purification system was employed in the experiment for solution preparation.

2.2. The preparation of adsorbents

The biochar loaded with iron and zinc (Fe/Zn-biochar) was prepared by a one-step synthesis method as follows. First, the mixture of 15 g sawdust and the solution containing 0.2354 g $ZnCl_2$, 0.72321 g $FeCl_3\ 6H_2O$ and 150 mL water was stirred for 24 h, and the multicomponent mixture was kept at 100 °C for 48 h. Then, the aqueous solution containing 0.2354 g $ZnCl_2$, 0.5424 g $FeCl_3\ 6H_2O$ and 150 mL water was repeatedly added to the above sample, and treated as described above to increase the iron and zinc oxide loading amount. Finally, the pretreated sawdust was calcined at 600 °C for 2 h with a heating rate of 5 °C/min in the tube furnace under nitrogen flow.

For comparison, single iron or zinc modified biochar (Fe-biochar, Zn-biochar) and a pristine biochar (P-biochar) were prepared by the same method of Fe/Zn-biochar preparation, while an equal amount of iron source, zinc source or none, respectively was added to the biochar for their preparation in the impregnation procedures.

2.3. Material characterization

Scanning electron microscope (SEM) images obtained on a Hitachi S4800 were applied to present the surface morphology of the materials. The apparent surface area and pore volume of the adsorbents were ascertained using the nitrogen adsorption-desorption isotherms conducted on a Micromeritics 2020 analyzer at 77 K. X-ray diffraction patterns were conducted on an X-ray diffractometer (Rigaku D/max-2500, Japan). Fourier transform infrared spectrometer (FTIR, Nicolet Magna-IR 750) was applied to detect the existing surface functional groups on the adsorbents. The element composition on the material surface was analyzed by the X-ray photoelectron spectroscopy (XPS, Thermo Fisher Scientific, UK). The zeta potentials of the materials were measured on a Zetasizer Nano (ZEN3600, Malvern). And the magnetization of Fe/Zn-biochar was confirmed on a Vibrating sample magnetometer (Quantum Design MPMS-XL-7).

2.4. Batch experiments

To investigate the effects of various parameters including initial solution pH, reaction time, initial concentration, temperature and ionic strength on PNP adsorption by the prepared adsorbents, the batch experiments were conducted. In the process of each experiment, 15 mL prepared PNP solution was put into a 50 mL conical flask with 15 mg adsorbent added, which was shaken for a fair amount of time at 150 rpm at 25 °C unless otherwise stated, and the initial solution pH values were adjusted using NaOH or HCl solution. At the end of the reaction, the adsorbent and the solution was separated by magnet or centrifugation, and the concentration of residual PNP was measured by UV–vis spectrophotometer (Shimadzu, UV-2550, Japan) in alkaline form at wavelength of 400 nm or acidic form at wavelength of 318 nm [25,26]. As for Pb(II), its concentration was determined by a Perkin–Elmer Analyst 700 atomic absorption spectrophotometer (AAS, Perkin-Elmer, USA). The equations to calculate adsorption capacity (q_t, mg/g) and removal percentage (R, %) for PNP or Pb(II) were listed in Text S1, Supporting information.

3. Results and discussion

3.1. Characterization

To obtain the surface morphology of the adsorbents, the SEM characterization of P-biochar, Fe/Zn-biochar, Fe-biochar and Zn-biochar was carried out. In Fig. 1a, the SEM figure of P-biochar implied that the sawdust was fully carbonized, and tiny carbon sticks or slices existed on the surface of the P-biochar. An evident difference could be observed on the SEM figures of modified biochar from Fig. 1b–d, some crystal particles were evenly distributed on the surface of metal doped biochar. The particles probably were the generated iron oxides or zinc oxides during the pyrolysis process, which indicated the successful preparation of the adsorbent and may contribute to the increased surface area and pore volume.

The nitrogen adsorption-desorption isotherms were conducted on P-biochar, Fe-biochar, Zn-biochar and Fe/Zn-biochar. The apparent surface area calculated by Brunauer–Emmett–Teller (BET) method, pore volume and average pore calculated by Barrett–Joyner–Halenda (BJH) method of the P-biochar and modified biochar were shown in Table S1. It was evident that the P-biochar possessed high apparent surface area (435.23 m^2/g), and

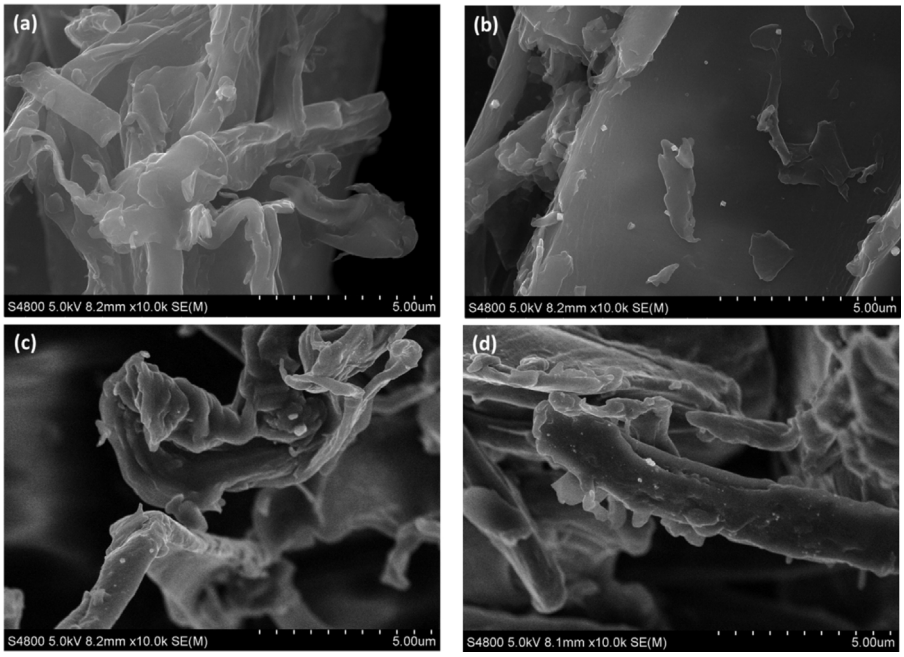

Fig 1. SEM images of (a) P-biochar, (b) Fe/Zn-biochar, (c) Fe-biochar, (d) Zn-biochar.

after the introduction of iron or/and zinc to the biochar, both of the apparent surface area and pore volume of the modified biochar with microporous structure increased a bit, which may be attributed to the distribution of metal oxides particles on the surface and the enlargement of the pore structure of the materials by the metal oxides particles entering into the pores [27]. It was beneficial for contamination removal.

The FTIR spectra of P-biochar, Fe-biochar, Zn-biochar, Fe/Zn-biochar and PNP adsorbed Fe/Zn-biochar were presented in Fig. 2A. There are five common characteristic peaks centered at about 3439 cm^{-1} (O—H), 2942 cm^{-1} (CH—), 1569–1625 cm^{-1} (C=C), 1384 cm^{-1} (COO^-), and 1095 cm^{-1} (C—O) in their spectra [28]. The broad peak at 1585 cm^{-1} corresponding to C=C vibration in P-biochar spectrum shifted a bit in the spectra of the other three fresh adsorbents (about 1625 cm^{-1}), which might be ascribing to the addition of iron and/or zinc in the modified biochar [29]. The new peak centered at about 582 cm^{-1} generated in Fe-biochar and Fe/Zn-biochar was attributed to Fe–O stretch vibration, implying that the iron was successfully doped in the relative adsorbents [30]. In addition, comparing with the FTIR spectrum of Fe/Zn-biochar before and after PNP adsorption, a new characteristic peak at 818 cm^{-1} was found in spent Fe/Zn-biochar and it might be ascribing to the C—H out of plane vibration on the benzene ring [12]. And the peaks centered at 1384 cm^{-1} (COO^-), 1625 cm^{-1} (C=C) and 3419 cm^{-1} (O—H) in fresh Fe/Zn-biochar shifted to 1398 cm^{-1}, 1569 cm^{-1} and 3439 cm^{-1} respectively in PNP adsorbed Fe/Zn-biochar, which indicated that these groups may get participated in the PNP adsorption reaction.

In order to further confirm the crystalline phase formed on Fe-biochar, Zn-biochar and Fe/Zn-biochar, the modified biochar were analyzed by the XRD, and the wide-angle XRD patterns were shown in Fig. 2B. It could be speculated that zinc in Zn-biochar predominantly exists as hexagonal phase ZnO (JCPDS card No. 36-1451). While iron in Fe-biochar exist mainly in three main forms, as cubic phase Fe_3O_4 (JCPDS card No. 65-3107), cubic phase FeO (JCPDS card No. 06-0615) and orthorhombic phase Fe_3C (JCPDS card No. 35-0772), respectively. In addition, from the XRD pattern of Fe/Zn-biochar, the peaks centered at 2θ = 18.1°, 29.9°, 35.3°, 36.9°, 42.9°, 53.2°, 56.7°, 62.3°, 70.6°, and 73.6° were agreed well with 111,

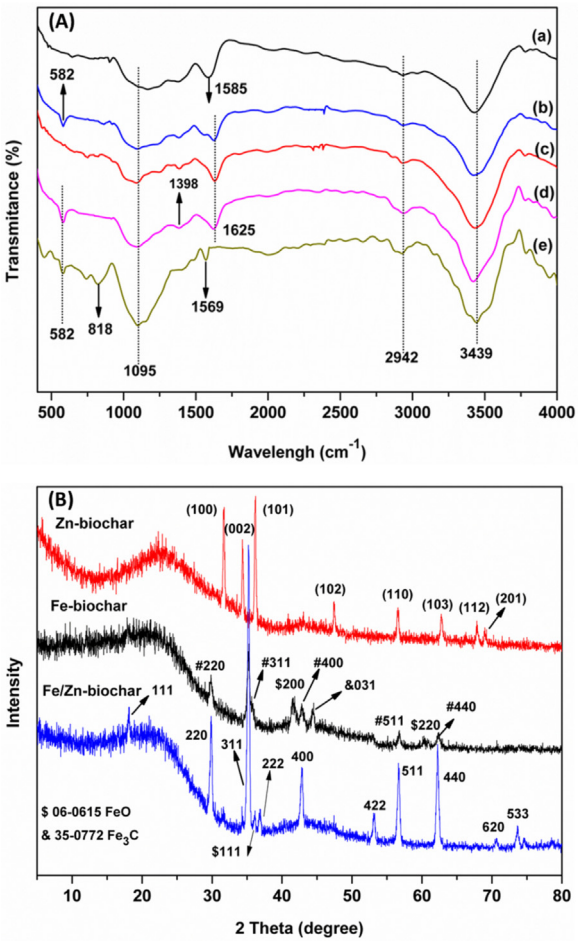

Fig. 2. (A) The FTIR spectra of (a) P-biochar, (b) Fe-biochar, (c) Zn-biochar, (d) Fe/Zn-biochar, and (e) PNP adsorbed Fe/Zn-biochar. (B) The XRD patterns of Fe/Zn-biochar, Zn-biochar and Fe-biochar.

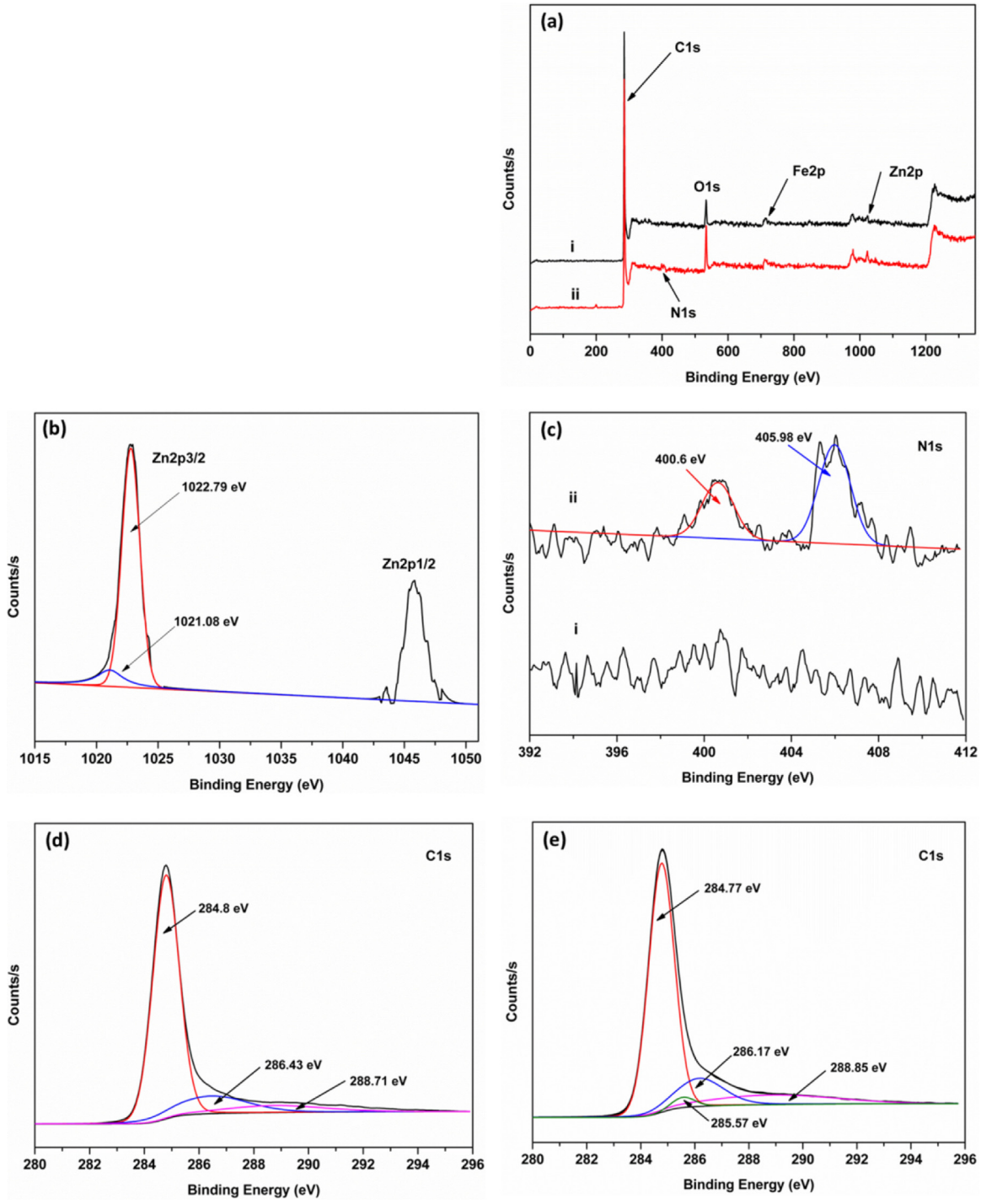

Fig. 3. XPS full scans (a) of Fe/Zn-biochar before (i) and after (ii) adsorption; Zn2p XPS spectrum (b) of Fe/Zn-biochar; N1s XPS spectrum (c) of PNP adsorbed Fe/Zn-biochar; C1s XPS spectra of Fe/Zn-biochar before (d) and after (e) PNP adsorption.

220, 311, 222, 400, 422, 440 and 533 reflections of cubic phase Fe_2ZnO_4 (JCPDS card No. 22-1012) or cubic phase Fe_3O_4 (JCPDS card No. 65-3107). The rest peak at 36.142° was corresponded to cubic phase FeO (JCPDS card No. 06-0615). It indicated that the metal species of iron and zinc on the prepared Fe/Zn-biochar were predominantly magnetic Fe_2ZnO_4 (Fe_2O_3/ZnO) [31,32], Fe_3O_4, and FeO, respectively.

The XPS spectra of fresh Fe/Zn-biochar and spent Fe/Zn-biochar after adsorbing PNP were shown in Fig. 3a. The full scan spectrum of the Fe/Zn-biochar showed the existence of C1s (92.62%), O1s (5.89%), Fe2p and Zn2p peaking at binding energies of 284.79, 533.56, 711.88 and 1022.15 eV, respectively. The low ratio of O/C indicated the low amount of oxygen-containing groups on Fe/Zn-biochar, and the presence of Fe and Zn in fresh Fe/Zn-biochar indicated that the zinc and iron was successfully introduced to the Fe/Zn-biochar. As for the PNP adsorbed Fe/Zn-biochar, a new peak centered at 405.97 eV corresponding to N1s was generated in its XPS spectrum.

The detailed XPS spectra of the region for C1s, N1s, Zn2p were analyzed and presented in Fig. 3b–e. As can be seen, two new peaks at 400.6 eV, 405.98 eV were generated in N1s spectrum of spent Fe/Zn-biochar, which was corresponded to C—N and nitro groups

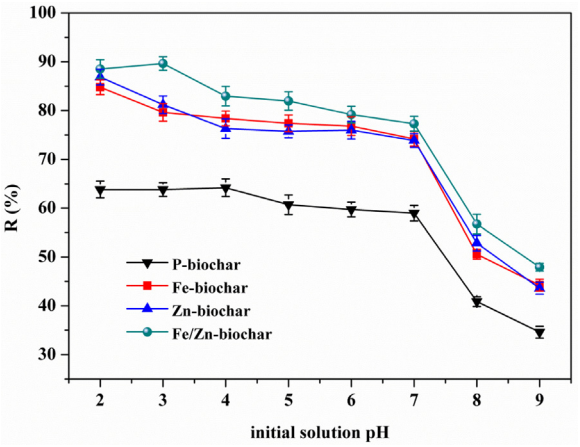

Fig. 4. The effect of initial solution pH on PNP adsorption by pristine and modified biochar (initial PNP concentration of 150 mg/L, at 25 °C).

from PNP [7,21], so it could be speculated that the emergence of N in spent Fe/Zn-biochar was due to the adsorbed PNP. There were two evident peaks in Zn2p spectrum of fresh Fe/Zn-biochar centered at about 1022.8 and 1045.8 eV ascribing to the peaks of Zn2p3/2 and Zn2p1/2, and another two significant peaks centered at 1021.08 and 1022.8 eV which were decomposed by the peak of Zn2p3/2 may be corresponded to zinc oxide and zinc hydroxide [33,34].

In Fig. 3d, the C1s spectrum of fresh adsorbent was decomposed into three peaks, attributing to 284.8 eV (C=C/C—H), 286.43 eV (C—O) and 288.71 eV (COO^-), respectively [35]. While in the C1 s spectrum of the spent adsorbent, the above three relative peaks, 284.77 eV (C=C/C—H), 286.17 eV (C—O) and 288.85 eV (COO^-), could also be observed. Furthermore, there was a newborn peak centered at 285.57 eV assigned to C—N [13], which was consistent with the result in N1s spectrum.

3.2. Effect of solution pH

Solution pH was a vital factor affecting the adsorption effect since it both determined both the degree of the dissociation of the adsorbate and the surface charge of the adsorbent [30,36]. The zeta potentials of the pristine and modified biochar were shown in Fig. S1, and the difference among them may be ascribing to the introduction of iron and/or zinc. The zero potential point (pH_{zpc}) of P-biochar and Fe/Zn-biochar was about 4.47 and 4.06. When solution pH was lower than the critical point, the surface of the material was protonated and its surface charge was positive, otherwise, it was the opposite.

The inset of Fig. S1 was the VSM measurement of Fe/Zn-biochar, its saturation magnetism was 2.85 emu g^{-1} which was beneficial for magnetic separation [37]. After adsorption reaction, the adsorbent could be separated from the aqueous solution by using a magnet.

Furthermore, the effect of initial solution pH on the removal efficiency of P-biochar, Fe-biochar, Zn-biochar, and Fe/Zn-biochar for PNP were carried out by varying the solution pH from 2 to 9, and the results were shown in Fig. 4. It could be found out that the overall trend of the impact of initial solution pH on PNP adsorption was similar using the above four adsorbents respectively, the PNP adsorption decreased with the increased solution pH, which was consistent with the result from Park et al. [38]. Furthermore, comparing with the P-biochar, the modified biochar adsorbents showed better adsorption effect for PNP and it may be due to their higher apparent surface area, larger adsorbent pore size, as well as the low amount of hydroxyl groups formed on zinc oxide on the adsorbents. From the different PNP removal efficiencies among the modified biochar adsorbents, it indicated that in addition to their different surface areas, their pore size could also affect their PNP adsorption performance. Additionally, the molecular size of PNP was estimated to be about 0.75 nm, and a suitable pore size of the adsorbent was thought to be about twice the size of PNP molecules [39]. Thus, the Zn-biochar and Fe/Zn-biochar adsorbents with larger pore size were beneficial for diffusion of PNP into the micro-pores of biochar [4,40].

At low solution pH, the PNP was mainly in molecular form whose pKa value was 7.15, and the adsorption of PNP was ascribing to the hydrophobic interaction, hydrogen bond between the nitro, hydroxyl groups in PNP molecules and hydroxyl, carboxyl groups on adsorbent surface, and dispersion interaction between the aromatic ring and the basal planes of Fe/Zn-biochar [4,5,38,41,42]. And if the hydrogen bond was the main interaction among them, the maximum PNP adsorption amount should occur at a pH value around pHzpc. However, the optimized solution pH for PNP adsorption was at a lower pH there [43]. As for the π-π dispersion interaction, the small amount of oxygen-containing groups on the surface of Fe/Zn-biochar and the electron-withdrawing $-NO_2$ in PNP decreased the electron density of the basal planes and aromatic ring, leading to a weaker dispersion interaction [4,44]. So, the hydrophobic interaction might be predominant here.

When pH > pH_{zpc}, the surface of the material was deprotonated, and with the increase of solution pH, especially while raised to neutral or alkaline conditions, a larger portion of PNP was ionized. A sharp decrease of PNP adsorption amount from pH 7 to 9 resulted from the electrostatic repulsion, which played a vital role in the reaction between the ionized PNP and adsorbent with negatively charged surface.

Furthermore, it could be observed that the Fe/Zn-biochar obtained the maximum removal efficiency for PNP (90%) at pH 3, and thus other experiments to perform PNP adsorption by the material were conducted at pH 3.

3.3. Effect of contact time and adsorption kinetics

The effect of reaction time on PNP removal for the initial concentration of 150 mg/L by the modified and pristine biochar conducted at pH 3 and 25 °C was depicted in Fig. 5a. It was noteworthy that the adsorption of PNP onto pristine and modified biochar was a time-dependent process, and the adsorption rate of PNP by Fe/Zn-biochar was the fastest among the four materials. The rapid initial adsorption stage might be due to the hydrophobic interaction between the biochar and the PNP molecules [43], and especially, the adsorption of PNP rapidly occurred in the first 7 h accounted for 80% of the total adsorption capacity, then, followed by a slower adsorption process until it reached equilibrium at 30 h.

To help analyze the reaction mechanism, the adsorption kinetics were investigated. The Pseudo-first-order and Pseudo-second-order model were applied to fit the experiment data respectively, and the equations were presented in Text S2, Supporting information.

The fitting result of the two kinetic models was depicted in Table 1, and it could be clearly concluded that the experimental data fitted well with the Pseudo-second-order model due to its higher correlation coefficient values (R^2 = 0.92) and much closer theoretical q_e value to the experimental q_e value when comparing with the former kinetic model. To further analyze the diffusion mechanism, the intra-particle diffusion model was applied, and its equation was described in Text S2, Supporting information. The plot of q_t versus $t^{0.5}$ was presented in Fig. 5b. Evidently, three line segments were contained in the plots and they represented three different stages in adsorption process. Firstly, at the first stage, the sharper-sloped portion represented the adsorption of PNP onto the external surface of the adsorbent, and especially, at this stage, nearly 70% PNP

Table 1
Parameters of Pseudo-first-order model and Pseudo-second-order equation model for PNP adsorption onto the pristine and modified biochar.

Adsorbents	Pseudo-first-order			Pseudo-second-order		
	q_e (mg/g)	k_1 (min^{-1})	R^2	q_e (mg/g)	k_2 (g/mg min)	R^2
Fe/Zn-biochar	128.15	0.241	0.815	137.46	0.000117	0.936
Fe-biochar	99.68	0.022	0.777	107.02	0.000139	0.917
Zn-biochar	110.16	0.013	0.83	120.3	0.000068	0.907
P-biochar	83.17	0.01	0.828	91.47	0.000072	0.929

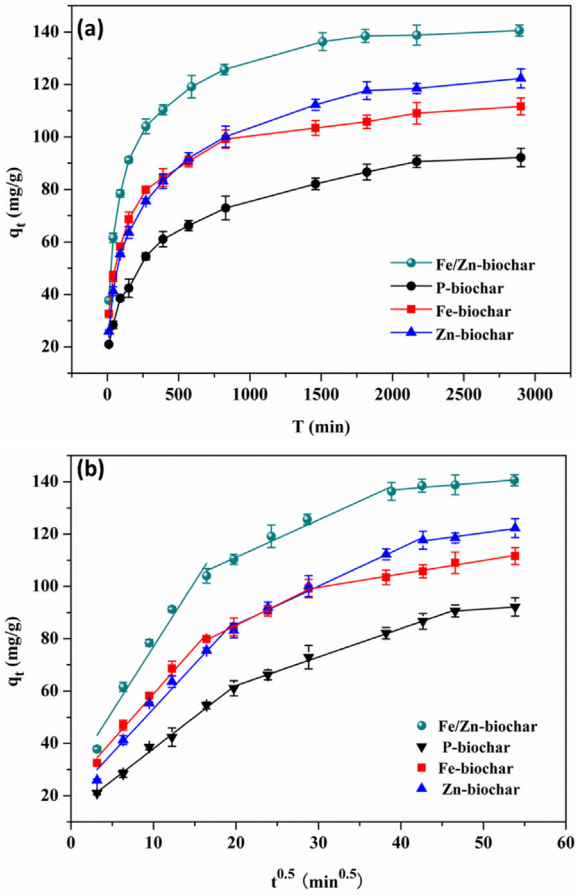

Fig. 5. Effect of contact time (a) and (b) intra-particle diffusion contact time on PNP adsorption by pristine and modified biochar.

molecules in the solution were adsorbed onto the external surface of Fe/Zn-biochar, so the adsorption of PNP occurred on the external surface of the biochar was significant. Secondly, the centered portion stood for that the PNP diffused to the pores of the modified biochar and adsorbed by its internal surface of the pores. Lastly, the platform stage suggested that the intra-particle diffusion slowed down and reached adsorption equilibrium. Due to the slower adsorption rate during the latter two stages, the rate limiting stage might be the intra-particle diffusion [45,46].

3.4. Sorption isotherm and thermodynamic studies

The adsorption isotherms studies were applied to investigate the reaction behavior between the solid material and the PNP molecules. In the study, the adsorption isotherms were conducted at 25 °C with initial PNP concentration varying from 10 to 500 mg/L at pH 3 by Fe/Zn-biochar, Fe-biochar, and Zn-biochar, respectively. Here, the Langmuir isotherm model and Freundlich isotherm model were selected to fit the experiment data respectively, and the results were shown in Fig. 6. The Langmuir isotherm model is set

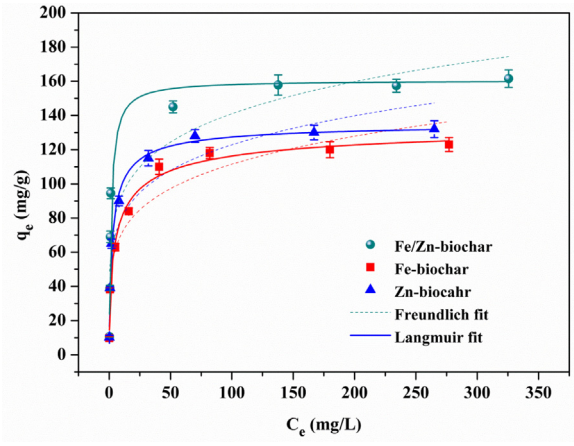

Fig. 6. The Adsorption isotherms of adsorption PNP onto Fe/Zn-biochar, Fe-biochar and Zn-biochar, respectively.

Table 2
Parameters of Langmuir and Freundlich models for PNP adsorption onto Fe/Zn-biochar.

Adsorbents	Langmuir			Freundlich		
	K_L (L/mg)	q_m (mg/g)	R^2	K_F	n	R^2
Fe/Zn-biochar	0.771	157.98	0.965	61.43	5.54	0.842
Fe-biochar	0.251	122.2	0.95	44.92	5.05	0.898
Zn-biochar	0.485	134.5	0.979	52.02	5.36	0.864

up based on the hypothesis that all sites were equal and no reaction occurred among the adsorbed molecules, while the Freundlich isotherm model describes that the binding sites were not equal and the adsorption occurred on a heterogeneous surface from extensive experience. The equations are expressed in Text S3, Supporting information.

In addition, the separation factor (R_L) based on the Langmuir model was used to evaluate the adsorption process, and it was defined in Text S3, Supporting information.

The results about the relevant parameters calculated from the above two isotherm model were shown in Table 2. It was evident that comparing with the Freundlich model, the Langmuir model fitted the experiment data better in view of their higher correlation coefficient R^2. Thus, based on the Langmuir model, the maximum adsorption capacities for PNP at 25 °C by Fe/Zn-biochar, Zn-biochar and Fe-biochar were about 158, 134.5, 122.2 mg/L, respectively. And the application of the Langmuir model suggested that the homogeneous and monolayer adsorption of PNP occurred on the adsorbents ascribing to the evenly distributed adsorption sites on its surface. Furthermore, while K_L >0, the value of separation factor R_L was between 0 and 1, so the adsorption of PNP onto Fe/Zn-biochar was evaluated favorable.

The adsorption thermodynamic studies were conducted at 298.15 K, 308.15 K, 318.15 K, respectively to evaluate the adsorption reaction. Three thermodynamic parameters, the free energy change (ΔG, kJ/mol), the enthalpy change (ΔH, kJ/mol), the entropy change (ΔS, kJ/K mol) were applied to describe the adsorption pro-

Table 3
Thermodynamic parameters for the adsorption of PNP by Fe/Zn-biochar at different temperatures.

T (K)	ΔG (kJ/mol)	ΔH (kJ/mol)	ΔS (kJ/K mol)
298.15	−0.331	4.35	0.0157
308.15	−0.488		
318.15	−0.645		

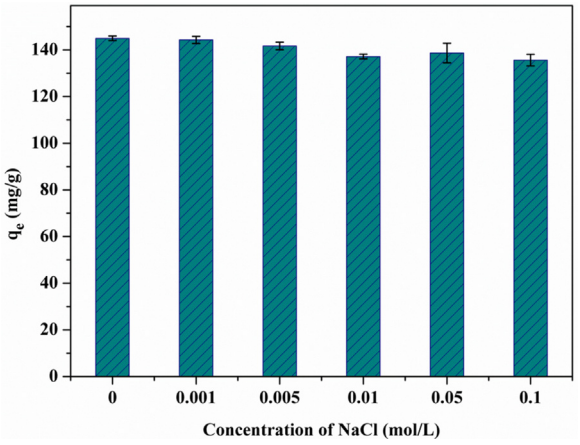

Fig. 7. Effect of ionic strength (NaCl) on PNP adsorption by Fe/Zn-biochar.

cess, and they were determined by the equations listed in Text S4, Supporting information.

The result was depicted in Table 3. The negative values of ΔG and positive ΔH indicated that the process of PNP adsorption by Fe/Zn-biochar was a spontaneous and endothermic reaction, and the small absolute value of ΔH (4.35 kJ/mol) suggested that the physisorption might be a dominant step in the adsorption process of PNP onto Fe/Zn-biochar [20]. Furthermore, the positive value of ΔS indicated the affinity between the PNP and Fe/Zn-biochar and implied an increasing randomness during the adsorption process on the solid- solution interface.

3.5. *Effect of ionic strength*

Given that common ions often existed in wastewater, the effect of ionic strength on the adsorption of PNP was carried out here by adjusting the additive amount of sodium chloride from 0 to 0.1 mol/L. The relative result was presented in Fig. 7, and it showed that the PNP adsorption amount decreased slightly with the increased concentration of NaCl. At pH 3, the predominant interaction between PNP molecules and the modified biochar was the non-electrostatic interactions, the hydrophobic interaction, and it was inferred that the increased concentration of NaCl could lead to the decreased solubility of PNP which was beneficial for PNP adsorption [5,16,22]. However, the negative effect of salt on PNP adsorption might be due to the competition for space in adsorbent between the PNP and NaCl [43].

3.6. *The simultaneous removal of Pb(II) and PNP*

The phenolic compounds and heavy metals commonly coexist in printing, agricultural irrigation, etc. and may cause more heavy damage to the environment due to their mutual effect [21,24,47,48], so the simultaneous removal of them was essential.

3.6.1. *The single system for Pb(II) adsorption*

To obtain the essential adsorption characteristics and to help analyze the adsorption mechanism for Pb(II) by Fe/Zn-biochar, the batch experiments for Pb(II) adsorption were conducted to found

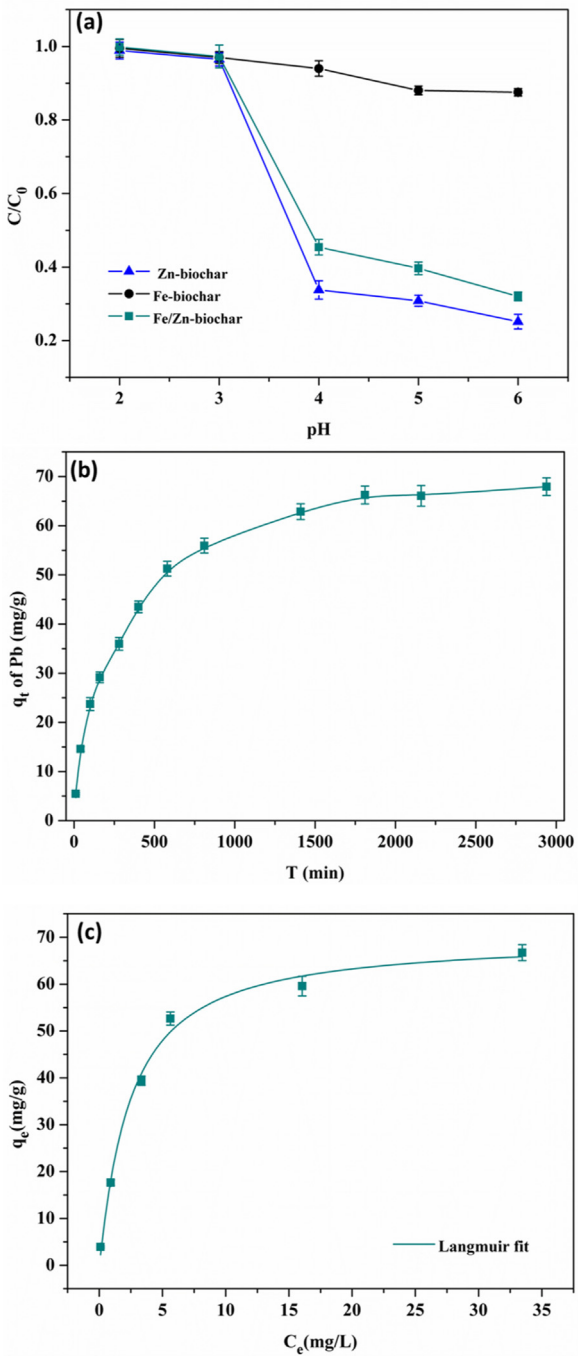

Fig. 8. (a) Effect of solution pH on Pb(II) adsorption by Fe/Zn-biochar, Fe-biochar and Zn-biochar, and (b) effect of contact time on Pb(II) adsorption by Fe/Zn-biochar at 25 °C, (Pb(II) solution concentration and volume: 100 mg/L, 20 mL; adsorbent dosage: 20 mg) (c) the adsorption isotherm for Pb(II) onto Fe/Zn-biochar.

out the effect of solution pH and contact time on Pb(II) adsorption as well as its adsorption isotherm type.

To avoid the precipitation of Pb(II), the experiments were conducted for Pb(II) adsorption by Fe-biochar, Zn-biochar and Fe/Zn-biochar respectively with solution pH range from 2 to 6, and the results were presented in Fig. 8a. It could be observed that the Fe doped biochar showed low adsorption capacity for Pb(II) under all pH conditions conducted which might result from the poorly developed structure of the biochar in the study and the low affinity of Pb(II) to sorb on iron oxides [49]. While the removal efficiency of Pb(II) by Fe/Zn-biochar reached 68% at pH 6, and the Zn-biochar pre-

sented a little better adsorption performance for Pb(II) compared with Fe/Zn-biochar (76%). It indicated that the addition of zinc to biochar was helpful for the adsorption of Pb(II), which might be due to the generated hydroxyl groups on the zinc oxide on Fe/Zn-biochar [9,50]. And the better adsorption performance for Pb(II) by Zn-biochar compared with Fe/Zn-biochar might be attributed to a little more zinc oxides as well as hydroxyl groups formed on Zn-biochar while an equal initial amount of zinc source added in the preparation process of the adsorbents. Moreover, the adsorption capacities for Pb(II) by Fe/Zn-biochar and Zn-biochar were increased from pH 3 to 6. Due to that the pH_{zpc} of the two kinds of adsorbents were around 4, with the increase of solution pH, electrostatic attraction generated between the cationic Pb(II) and the negatively charged adsorbent was beneficial for Pb(II) adsorption.

The effect of reaction time on Pb(II) adsorption by Fe/Zn-biochar was shown in Fig. 8b, with the whole reaction continuing for 48 h. It could be observed, in the first 10 h, about 51% of the total Pb(II) in solution was adsorbed, then, a slower adsorption process was followed, and the adsorption reaction reached equilibrium at about 30 h with 68% Pb(II)removed.

As shown in Fig. 8c, the adsorption type of Pb(II) adsorption onto Fe/Zn-biochar could be well described by the Langmuir isotherm model ascribing to its high correlation coefficient (R^2 = 0.989), indicating the monolayer adsorption for Pb(II) on the adsorbent, and it was consistent with the result obtained by the earlier researcher [50].

3.6.2. The coexistence of Pb(II) and PNP

To evaluate the effect of the simultaneously existing of PNP and Pb(II) on the adsorption of single contaminant of them onto Fe/Zn-biochar, the binary adsorption experiments were conducted by fixing Pb(II) concentration and varying PNP concentration from 10 to 300 mg/L at pH 6, and the results were shown in Fig. 9. From Fig. 9a, it could be observed that the presence of Pb(II) at 10 mg/L, 35 mg/L and 73 mg/L, respectively could slightly promote the PNP adsorption by comparison with the single PNP adsorption system with no Pb(II) addition, and the promoted PNP adsorption might be ascribing to the formed PNP–Pb(II) complex. Furthermore, under the same initial PNP concentration, the PNP adsorption capacity decreased when the coexisting Pb(II) concentration increased from 35 to 73 mg/L. It indicated that the complexation interaction between Pb(II) and PNP occurred only in a small portion, and greater competitive adsorption between them for adsorption sites on Fe/Zn-biochar existed at higher Pb(II) concentration. While the concentration of Pb(II) was 110 mg/L, the competitive adsorption between them predominated, and the PNP adsorption was suppressed [51].

The influence of coexisting PNP on the adsorption capacity of Pb(II) onto Fe/Zn-biochar could be indicated based on the variation trend of the numerical difference between the initial Pb(II) concentration and the Pb(II) adsorption capacity in single and binary system, which was equal to the residual concentration of Pb(II) in solution ascribing to 1 g/L adsorbent mass. From Fig. 9b, it could be observed that when Pb(II) was 10 mg/L, it was nearly removed thoroughly by Fe/Zn-biochar in both single and binary system. When Pb(II) concentration increased to 35 mg/L, the coexisted low concentration of PNP (from 10 to 70 mg/L) could slightly facilitate the Pb(II) adsorption with little residual Pb(II) in solution in binary system comparing with that (about 3 mg/L) in single system. While the initial Pb(II) concentration further increased to 73 mg/L, the adsorption capacity of Pb(II) by Fe/Zn-biochar increased about 5.5 mg/L in presence of 20 mg/L PNP comparing with that in single system, and the promoted adsorption is not obvious when the PNP increased to 70 mg/L. With the further increase of coexisting PNP concentration, the growing residual Pb(II) concentration in solution indicated the suppressed Pb(II) adsorption by Fe/Zn-biochar.

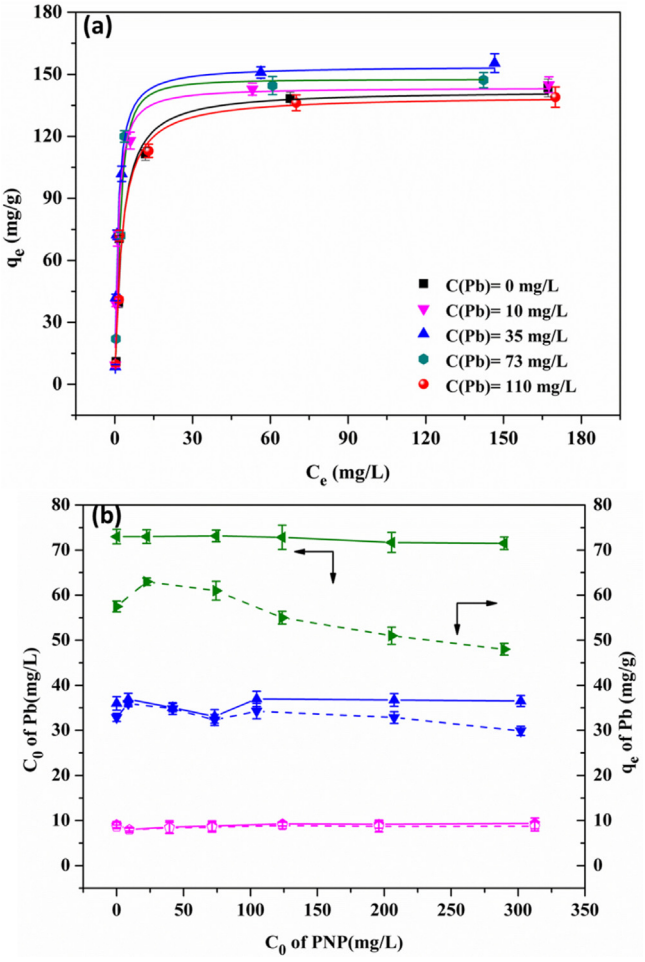

Fig. 9. (a) The Langmuir fit of PNP adsorption with/without Pb(II) addition and (b) the effect of PNP on Pb(II) adsorption by Fe/Zn-biochar (the solid line represents the C_0 of Pb(II), the dash line represents the q_e of Pb(II)).

3.6.3. Mechanism analysis for binary adsorption system

The adsorption mechanism for PNP and Pb(II) adsorption onto Fe/Zn-biochar was proposed based on all information obtained above. From their single adsorption system conducted above, it could be deduced that the PNP was adsorbed mainly by hydrophobic sites on Fe/Zn-biochar, while Pb(II) might be mainly adsorbed by the oxygen-containing hydrophilic sites on the adsorbent. By comparison with single adsorption system, new adsorption pathways might exist in binary adsorption system. The complex formed between Pb(II) and hydroxyl of PNP might chelate with hydroxyl, carboxyl groups on the adsorbent or be directly adsorbed on it. Furthermore, the complexation might also occur between the adsorbed PNP and free Pb(II) as well as the adsorbed Pb(II) and free PNP [24]. Thus, the increased adsorption of PNP at their low concentration might contribute to more PNP being adsorbed on Fe/Zn-biochar through the complexing-bridging mechanism, due to the stronger affinity between Pb(II) and hydroxyl, carboxyl groups on the adsorbent comparing with PNP. As for the enhanced adsorption for Pb(II), it might be due to the direct adsorption of the complex onto the hydrophobic sites on Fe/Zn-biochar [48]. And the main interaction among PNP, Pb(II), and Fe/Zn-biochar proposed in binary adsorption system was shown in Fig. 10. While at high concentration of Pb(II) and PNP, the great competition between

Table 4
The comparison of removal performance of various adsorbents for PNP removal.

Adsorbent	q_m (mg/g)	Isotherm model	Adsorption condition	Main adsorption mechanism	Refs
Carrot dross based AC	125	Langmuir model	pH = 3.5–4.5 T = 23–25 °C	Hydrogen bond	[4]
Carbon nanospheres	20	/	pH = 3	π-π interaction	[22]
FAU Zeolite	146	Fowler-guggenheim	pH = 4	Hydrophobic interaction	[23]
Organo-palygorskites	42.1	Freundlich model	pH = 6 T = 23 °C	Anion exchange	[25]
Mansonia sawdust	21.3	Langmuir model	pH = 4 T = 22–30 °C	Pore and film diffusion	[45]
Cocoa shell based AC	167	Langmuir model	pH = 7 T = 30 °C	π-π dispersion interaction	[39]
Fe/Zn-biochar	170	Langmuir model	pH = 3 T = 45 °C	Hydrophobic interaction	This study

Table 5
The comparison of removal performance of various adsorbents for Pb(II) removal.

Adsorbent	q_m (mg/g)	Isotherm model	Adsorption condition	Main adsorption mechanism	Refs
ZnO-GAC	45 mg/g (q_e)for 100 mg/L	Langmuir model	pH = 6	Chelation interaction	[50]
MWCNTs	17.5	Langmuir model	pH = 6 T = 20 °C	Outer-sphere and inter-sphere complexation	[52]
AC from phaseolus	21.8	Freundlich model	pH = 6 T = 30 °C	Electrostatic interaction	[53]
Silica/CA–XG	25.8	Langmuir model	T = 40 °C	Chelation with —OH, intra-particle diffusion	[54]
Fe/Zn-biochar	68 mg/g (q_e)for 100 mg/L	Langmuir model	pH = 6 T = 25 °C	Chelation between the hydroxyl on biochar and Pb(II)	This study

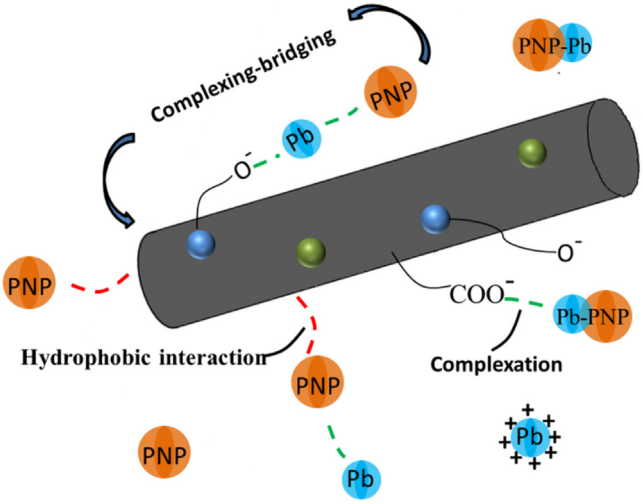

Fig. 10. The main interaction way among PNP, Pb(II), and Fe/Zn-biochar in binary adsorption system.

them for interaction with the adsorbent suppressed both of their adsorption.

3.7. The comparison with other studies

From mentioned above, it could be deduced that the total additive dosages of iron and zinc elements were about 1.75% and 1.5% of the quality of carbon source, respectively, calculated from the total additive dosages of iron and zinc source in the preparation of Fe/Zn-biochar, and it was really a small dosage. Furthermore, the carbon source was from the waste sawdust, a kind of abundant and low-cost raw materials. And the one-step synthesis method applied in the study needed less energy consumption compared with the post-synthesis method by impregnating the prepared biochar with metal. So, the Fe/Zn-biochar could be deduced as easily prepared and low-cost adsorbent.

The results in this study showed that while the two contaminants (Pb(II) and PNP) existed simultaneously in the system, the two types of adsorption sites (the hydrophobic and hydrophilic sites) on Fe/Zn-biochar could be fully applied for the contaminants removal. And there were previous studies for removal of Pb(II) and PNP by biochar or other adsorbents, compared with the studies by previous researchers, the Fe/Zn-biochar showed higher adsorption capacity for Pb(II) and PNP. The adsorption capacity (about 68 mg/g) for Pb(II) (100 mg/L) by Fe/Zn-biochar in this study was prevailing, while q_e for Pb(II) (100 mg/L) was 45 mg/g by ZnO-GAC [50], 17.5 mg/g by MWCNTs [52], 21.8 mg/g by Activated carbon [53], 18.9 mg/g by Silica/CA–XG [54]. As for PNP, the q_m value (170 mg/g) by Fe/Zn-biochar was larger than activated carbon from carrot dross (125 mg/g) [4], cocoa shell based AC (167 mg/g) [39] as well as other adsorbents like FAU Zeolite (146 mg/g) [23], mansonia wood sawdust (21.3 mg/g) [45], novel organopalygorskites (42.1 mg/g) [25], carbon nanospheres (20 mg/g) [22]. The details were shown in Tables 4 and 5, respectively. Moreover, the beneficial magnetism of Fe/Zn-biochar gave it a priority over those without magnetism due to its easy separation property. So it was a promising adsorbent for Pb(II) and PNP removal.

4. Conclusion

In this study, the Fe/Zn-biochar with large surface area was prepared and presented good performance for PNP removal. The results showed that the maximum adsorption capacity of PNP by Fe/Zn-biochar was 170 mg/g, and it could be affected by solution pH, ionic strength and temperature. The adsorption of PNP onto the adsorbent was mainly attributed to hydrophobic interaction. And the study of binary system reflected the partial chelation and competition interaction between PNP and Pb(II). Thus, the Fe/Zn-

biochar was a potential adsorbent for PNP and Pb(II) removal in wastewater due to its low cost, easy separation and excellent stability.

Acknowledgements

The study was financially supported by the National Program for Support of Top-Notch Young Professionals of China (2012), Projects 51579096, 51222805, 51521006 and 51508175 supported by National Natural Science Foundation of China, and the Program for New Century Excellent Talents in University from the Ministry of Education of China (NCET-11-0129), the Hunan Province Innovation Foundation for Postgraduate (CX2015B095).

Appendix A. Supplementary data

Supplementary data associated with this article can be found, in the online version, at http://dx.doi.org/10.1016/j.apsusc.2016.09.052.

References

[1] G.T. Li, W.Y. Zhu, C.Y. Zhang, S. Zhang, L.L. Liu, L.F. Zhu, W.G. Zhao, Effect of a magnetic field on the adsorptive removal of methylene blue onto wheat straw biochar, Bioresour. Technol. 206 (2016) 16–22.
[2] Y. Ding, Y.G. Liu, S.B. Liu, Z.W. Li, X.F. Tan, X.X. Huang, G.M. Zeng, Y.Y. Zhou, B.H. Zheng, X.X. Cai, Competitive removal of Cd(ii) and Pb(ii) by biochars produced from water hyacinths: performance and mechanism, RSC Adv. 6 (2016) 5223–5232.
[3] D. Mohan, A. Sarswat, Y.S. Ok, C.U. Pittman Jr., Organic and inorganic contaminants removal from water with biochar, a renewable, low cost and sustainable adsorbent-a critical review, Bioresour. Technol. 160 (2014) 191–202.
[4] T.R. Bastami, M.H. Entezari, Activated carbon from carrot dross combined with magnetite nanoparticles for the efficient removal of p-nitrophenol from aqueous solution, Chem. Eng. J. 210 (2012) 510–519.
[5] C. Moreno-Castilla, Adsorption of organic molecules from aqueous solutions on carbon materials, Carbon 42 (2004) 83–94.
[6] X.F. Tan, Y.G. Liu, G.M. Zeng, X. Wang, X.J. Hu, Y.L. Gu, Z.Z. Yang, Application of biochar for the removal of pollutants from aqueous solutions, Chemosphere 125 (2015) 70–85.
[7] G.X. Yang, H. Jiang, Amino modification of biochar for enhanced adsorption of copper ions from synthetic wastewater, Water Res. 48 (2014) 396–405.
[8] H. Noei, H.S. Qiu, Y.M. Wang, E. Loffler, C. Woll, M. Muhler, The identification of hydroxyl groups on ZnO nanoparticles by infrared spectroscopy, Phys. Chem. Chem. Phys. 10 (2008) 7092–7097.
[9] X.B. Wang, W.P. Cai, S.W. Liu, G.Z. Wang, Z.K. Wu, H.J. Zhao, ZnO hollow microspheres with exposed porous nanosheets surface: structurally enhanced adsorption towards heavy metal ions, Colloids. Surf. A Physicochem. Eng. Aspects 422 (2013) 199–205.
[10] J. Światowska-Mrowiecka, S. Zanna, K. Ogle, P. Marcus, Adsorption of 1,2-diaminoethane on ZnO thin films from p-xylene, Appl. Surf. Sci. 254 (2008) 5530–5539.
[11] Y.Y. Zhou, L. Tang, G.D. Yang, G.M. Zeng, Y.C. Deng, B.B. Huang, Y. Cai, J. Tang, J.J. Wang, Y.N. Wu, Phosphorus-doped ordered mesoporous carbons embedded with Pd/Fe bimetal nanoparticles for the dechlorination of 2,4-dichlorophenol, Catal Sci. Technol. 6 (2016) 1930–1939.
[12] B. Lai, Y.H. Zhang, Z.Y. Chen, P. Yang, Y.X. Zhou, J.L. Wang, Removal of p-nitrophenol (PNP) in aqueous solution by the micron-scale iron–copper (Fe/Cu) bimetallic particles, Appl. Catal. B Environ. 144 (2014) 816–830.
[13] L. Tang, J. Tang, G.M. Zeng, G.D. Yang, X. Xie, Y.Y. Zhou, Y. Pang, Y. Fang, J.J. Wang, W.P. Xiong, Rapid reductive degradation of aqueous p-nitrophenol using nanoscale zero-valent iron particles immobilized on mesoporous silica with enhanced antioxidation effect, Appl. Surf. Sci. 333 (2015) 220–228.
[14] S. Yi, W.Q. Zhuang, B. Wu, S.T.L. Tay, J.H. Tay, Biodegradation of p-Nitrophenol by aerobic granules in a sequencing batch reactor, Environ. Sci. Technol. 40 (2006) 2396–2401.
[15] A. Kumar, S. Kumar, S. Kumar, D.V. Gupta, Adsorption of phenol and 4-nitrophenol on granular activated carbon in basal salt medium: equilibrium and kinetics, J. Hazard. Mater. 147 (2007) 155–166.
[16] D.Y. Tang, Z. Zheng, K. Lin, J.F. Luan, J.B. Zhang, Adsorption of p-nitrophenol from aqueous solutions onto activated carbon fiber, J. Hazard. Mater. 143 (2007) 49–56.
[17] B. Lai, Z.Y. Chen, Y.X. Zhou, P. Yang, J.L. Wang, Z.Q. Chen, Removal of high concentration p-nitrophenol in aqueous solution by zero valent iron with ultrasonic irradiation (US-ZVI), J. Hazard. Mater. 250–251 (2013) 220–228.
[18] O. Gimeno, M. Carbajo, F.J. Beltran, F.J. Rivas, Phenol and substituted phenols AOPs remediation, J. Hazard. Mater. 119 (2005) 99–108.
[19] B. Bakheet, C.C. Qiu, S. Yuan, Y.J. Wang, G. Yu, S.B. Deng, J. Huang, B. Wang, Inhibition of polymer formation in electrochemical degradation of p-nitrophenol by combining electrolysis with ozonation, Chem. Eng. J. 252 (2014) 17–21.
[20] L. Tang, S. Zhang, G.M. Zeng, Y. Zhang, G.D. Yang, J. Chen, J.J. Wang, J.J. Wang, Y.Y. Zhou, Y.C. Deng, Rapid adsorption of 2,4-dichlorophenoxyacetic acid by iron oxide nanoparticles-doped carboxylic ordered mesoporous carbon, J. Colloid Interface Sci. 445 (2015) 1–8.
[21] T.P. Chen, F.Q. Liu, C. Ling, J. Gao, C. Xu, L.J. Li, A. Li, Insight into highly efficient coremoval of copper and p-nitrophenol by a newly synthesized polyamine chelating resin from aqueous media: competition and enhancement effect upon site recognition, Environ. Sci. Technol. 47 (2013) 13652–13660.
[22] J.C. Lazo-Cannata, A. Nieto-Márquez, A. Jacoby, A.L. Paredes-Doig, A. Romero, M.R. Sun-Kou, J.L. Valverde, Adsorption of phenol and nitrophenols by carbon nanospheres: effect of pH and ionic strength, Sep. Purif. Technol. 80 (2011) 217–224.
[23] B. Koubaissy, G. Joly, P. Magnoux, Adsorption and competitive adsorption on zeolites of nitrophenol compounds present in wastewater, Ind. Eng. Chem. Res. 47 (2008) 9558–9565.
[24] G.D. Yang, L. Tang, G.M. Zeng, Y. Cai, J. Tang, Y. Pang, Y.Y. Zhou, Y.Y. Liu, J.J. Wang, S. Zhang, W.P. Xiong, Simultaneous removal of lead and phenol contamination from water by nitrogen-functionalized magnetic ordered mesoporous carbon, Chem. Eng. J. 259 (2015) 854–864.
[25] B. Sarkar, Y.F. Xi, M. Megharaj, G.S.R. Krishnamurti, R. Naidu, Synthesis and characterisation of novel organopalygorskites for removal of p-nitrophenol from aqueous solution: isothermal studies, J. Colloid Interface Sci. 350 (2010) 295–304.
[26] Q.S. Liu, T. Zheng, P. Wang, J.P. Jiang, N. Li, Adsorption isotherm, kinetic and mechanism studies of some substituted phenols on activated carbon fibers, Chem. Eng. J. 157 (2010) 348–356.
[27] M.A.A. Zaini, R. Okayama, M. Machida, Adsorption of aqueous metal ions on cattle-manure-compost based activated carbons, J. Hazard. Mater. 170 (2009) 1119–1124.
[28] J.C. Tang, H.H. Lv, Y.Y. Gong, Y. Huang, Preparation and characterization of a novel graphene/biochar composite for aqueous phenanthrene and mercury removal, Bioresour. Technol. 196 (2015) 355–363.
[29] U. Suryavanshi, T. Iijima, A. Hayashi, Y. Hayashi, M. Tanemura, Fabrication of ZnO nanoparticles confined in the channels of mesoporous carbon, Chem. Eng. J. 179 (2012) 388–393.
[30] L. Tang, Z.H. Xie, G.M. Zeng, H.R. Dong, C.Z. Fan, Y.Y. Zhou, J.J. Wang, Y.C. Deng, J.J. Wang, X. Wei, Removal of bisphenol A by iron nanoparticle-doped magnetic ordered mesoporous carbon, RSC Adv. 6 (2016) 25724–25732.
[31] P. Brown, L.J. Hope-Weeks, The synthesis and characterization of zinc ferrite aerogels prepared by epoxide addition, J. Sol-Gel. Sci. Technol. 51 (2009) 238–243.
[32] D. Wang, Z.Q. Chen, D.D. Wang, J. Gong, C.Y. Cao, Z. Tang, L.R. Huang, Effect of thermal annealing on the structure and magnetism of Fe-doped ZnO nanocrystals synthesized by solid state reaction, J. Magn. Magn. Mater. 322 (2010) 3642–3647.
[33] C. Gan, Y.G. Liu, X.F. Tan, S.F. Wang, G.M. Zeng, B.H. Zheng, T.T. Li, Z.J. Jiang, W. Liu, Effect of porous zinc–biochar nanocomposites on Cr(vi) adsorption from aqueous solution, RSC Adv. 5 (2015) 35107–35115.
[34] V.M. Gun'ko, V.M. Bogatyrov, O.I. Oranska, I.V. Urubkov, R. Leboda, B. Charmas, J. Skubiszewska-Zięba, Synthesis and characterization of resorcinol–formaldehyde resin chars doped by zinc oxide, Appl. Surf Sci. 303 (2014) 263–271.
[35] H. Wang, X.Z. Yuan, Y. Wu, X.H. Chen, L.J. Leng, H. Wang, H. Li, G.M. Zeng, Facile synthesis of polypyrrole decorated reduced graphene oxide–Fe3O4 magnetic composites and its application for the Cr(VI) removal, Chem. Eng J. 262 (2015) 597–606.
[36] M. Ahmaruzzaman, D.K. Sharma, Adsorption of phenols from wastewater, J. Colloid Interface Sci. 287 (2005) 14–24.
[37] L. Tang, Y. Cai, G.D. Yang, Y.Y. Liu, G.M. Zeng, Y.Y. Zhou, S.S. Li, J.J. Wang, S. Zhang, Y. Fang, Y. He, Cobalt nanoparticles-embedded magnetic ordered mesoporous carbon for highly effective adsorption of rhodamine B, Appl. Surf. Sci. 314 (2014) 746–753.
[38] K.H. Park, M.S. Balathanigaimani, W.G. Shim, J.W. Lee, H. Moon, Adsorption characteristics of phenol on novel corn grain-based activated carbons, Micropor. Mesopor. Mater. 127 (2010) 1–8.
[39] A. Fisal, W.M.A.W. Daud, M.A. Ahmad, R. Radzi, Using cocoa (Theobroma cacao) shell-based activated carbon to remove 4-nitrophenol from aqueous solution: kinetics and equilibrium studies, Chem. Eng. J. 178 (2011) 461–467.
[40] M. Vithanage, S.S. Mayakaduwa, I. Herath, Y.S. Ok, D. Mohan, Kinetics, thermodynamics and mechanistic studies of carbofuran removal using biochars from tea waste and rice husks, Chemosphere 150 (2016) 781–789.
[41] G. Newcombe, M. Drikas, Adsorption of NOM onto activated carbon: electrostatic and non-electrostatic effects, Carbon 35 (1997) 1239–1250.
[42] M. Franz, H.A. Arafat, N.G. Pinto, Effect of chemical surface heterogeneity on the adsorption mechanism of dissolved aromatics on activated carbon, Carbon 38 (2000) 1807–1819.
[43] W. Wei, R. Sun, J. Cui, Z.G. Wei, Removal of nitrobenzene from aqueous solution by adsorption on nanocrystalline hydroxyapatite, Desalination 263 (2010) 89–96.
[44] A. Dabrowski, P. Podkoscielny, Z. Hubicki, M. Barczak, Adsorption of phenolic compounds by activated carbon–a critical review, Chemosphere 58 (2005) 1049–1070.

[45] A.E. Ofomaja, Kinetics and pseudo-isotherm studies of 4-nitrophenol adsorption onto mansonia wood sawdust, Ind. Crops. Prod. 33 (2011) 418–428.
[46] Y.Y. Liu, G.M. Zeng, L. Tang, Y. Cai, Y. Pang, Y. Zhang, G.D. Yang, Y.Y. Zhou, X.X. He, Y. He, Highly effective adsorption of cationic and anionic dyes on magnetic Fe/Ni nanoparticles doped bimodal mesoporous carbon, J. Colloid Interface Sci. 448 (2015) 451–459.
[47] W.W. Tang, G.M. Zeng, J.L. Gong, Y. Liu, X.Y. Wang, Y.Y. Liu, Z.F. Liu, L. Chen, X.R. Zhang, D.Z. Tu, Simultaneous adsorption of atrazine and Cu (II) from wastewater by magnetic multi-walled carbon nanotube, Chem. Eng. J. 211–212 (2012) 470–478.
[48] L.C. Fu, F.Q. Liu, Y. Ma, X.W. Tao, C. Ling, A. Li, C.D. Shuang, Y. Li, High-efficient technique to simultaneous removal of Cu(II), Ni(II) and tannic acid with magnetic resins: complex mechanism behind integrative application, Chem. Eng. J. 263 (2015) 83–91.
[49] L. Trakal, V. Veselska, I. Safarik, M. Vitkova, S. Cihalova, M. Komarek, Lead and cadmium sorption mechanisms on magnetically modified biochars, Bioresour. Technol. 203 (2016) 318–324.
[50] Y. Kikuchi, Q. Qian, M. Machida, H. Tatsumoto, Effect of ZnO loading to activated carbon on Pb(II) adsorption from aqueous solution, Carbon 44 (2006) 195–202.
[51] G.C. Chen, X.Q. Shan, Y.S. Wang, B. Wen, Z.G. Pei, Y.N. Xie, T. Liu, J.J. Pignatello, Adsorption of 2,4,6-trichlorophenol by multi-walled carbon nanotubes as affected by Cu(II), Water Res. 43 (2009) 2409–2418.
[52] X.M. Ren, D.D. Shao, S.T. Yang, J. Hu, G.D. Sheng, X.L. Tan, X.K. Wang, Comparative study of Pb(II) sorption on XC-72 carbon and multi-walled carbon nanotubes from aqueous solutions, Chem. Eng. J. 170 (2011) 170–177.
[53] M.M. Rao, D.K. Ramana, K. Seshaiah, M.C. Wang, S.W. Chien, Removal of some metal ions by activated carbon prepared from Phaseolus aureus hulls, J. Hazard. Mater. 166 (2009) 1006–1013.
[54] S. Zhang, F. Xu, Y.F. Wang, W.Z. Zhang, X.L. Peng, F. Pepe, Silica modified calcium alginate–xanthan gum hybrid bead composites for the removal and recovery of Pb(II) from aqueous solution, Chem. Eng J. 234 (2013) 33–42.